Closed-loop-controlled vortex shedding and vibration of a flexibly supported square cylinder under different schemes

M. M. Zhang, L. Cheng,[a] and Y. Zhou
Department of Mechanical Engineering, The Hong Kong Polytechnic University, Hung Hom, Kowloon, Hong Kong

(Received 21 July 2003; accepted 26 January 2004; published online 5 April 2004)

Different schemes were experimentally investigated of the closed-loop control of vortex shedding from a spring-supported square cylinder in cross flow. The control action was implemented through the perturbation of one cylinder surface, which was generated by three piezoelectric ceramic actuators, embedded underneath the surface and controlled by a proportional-integral-derivative controller. Three control schemes were investigated using different feedback signals, including the turbulent flow signal measured by a hot wire, flow-induced structural oscillation signal obtained by a laser vibrometer, and a combination of both signals. An investigation was conducted at the resonance condition, when the vortex-shedding frequency coincided with the natural frequency of the fluid-structure system. The flow and structural vibration were measured using particle image velocimetry, laser-induced fluorescence flow visualization, a laser Doppler anemometer, and a laser vibrometer. It was observed that the control scheme based on the feedback of both flow and structural oscillation led to the almost complete destruction of the Kármán vortex street and a reduction in the structural vibration, vortex shedding strength, and drag coefficient by 82%, 65%, and 35%, respectively, outperforming by far an open-loop control as well as the other two closed-loop schemes. [DOI: 10.1063/1.1687413]

I. INTRODUCTION

The control of vortex shedding from a bluff body and vortex-induced structural vibration is of fundamental interest as well as of practical significance. A variety of control techniques have been developed in the past, which can be roughly classified as passive and active controls. Passive techniques rely on modifying the geometry of bluff bodies, adding vortex generators, grooves, or riblets to bluff bodies to affect the formation of the vortex shedding,[1,2] requiring no external energy input to the flow–structure system. In contrast, active methods involve the input of energies via actuators to bring about desirable changes to the flow–structure system, using either independent external disturbance or a feedback-signal controlled system. The former is often referred to as the open-loop control, whereas the latter is called the closed-loop control. In both cases, the control performance strongly depends on activating mechanisms and, in the latter case, also on the control scheme used.

Typical examples of the open-loop control include acoustic excitation,[3] oscillating or rotating cylinders,[4–6] and surface bleeding.[7] Recently, Cheng *et al.*[8] investigated a novel perturbation technique using curved piezoceramic actuators embedded underneath the surface of a square cylinder to alter interactions between a flexibly supported cylinder and cross flow. Given a properly set perturbation frequency, both vortex shedding and vortex-induced vibration were significantly reduced as a result from actuator-generated surface perturbation. However, their technique, without the feedback of either flow or structural vibration information, suffered from two major drawbacks. First, the perturbation frequency range to achieve desired performance was relatively narrow. Second, the required perturbation amplitude was rather large, about 2.8% of the cylinder height or 25% of the vibration amplitude of the cylinder. These problems may be resolved if a closed-loop system is developed.

The choice of the feedback signal is crucial for the performance of a closed-loop system. Previous closed-loop techniques involving flow or flow-induced vibration control mostly have their feedback signals from flow, typically hot wire signals. See Ffowcs Williams and Zhao,[9] Roussopoulos,[10] Huang,[11] Berger,[12] Warui and Fujisawa,[13] Tokumaru and Dimotakis,[14] and Filler *et al.*[15] for examples. This scheme should work quite well provided flow is to be controlled. For the same token, one may consider the structural vibration signal to be ideal for the control of structural vibration, one example is Baz and Ro.[16] Zhang *et al.*[17] investigated the closed-loop control of vortex shedding and flow-induced vibration of a flexibly supported square cylinder in cross flow. Their feedback signal was provided by the streamwise fluctuating velocity measured by a hot wire. They have achieved an effective control of both vortex shedding and flow-induced vibration. However, the performance of their system was not significantly superior to the open-loop system used by Cheng *et al.*[8] One may surmise that their feedback signal was from flow only, containing no information on structural vibration or flow–structure interactions, and might not provide the optimum feedback signal to control fluid–structure interactions. This begs the question:

[a]Electronic mail: mmlcheng@polyu.edu.hk

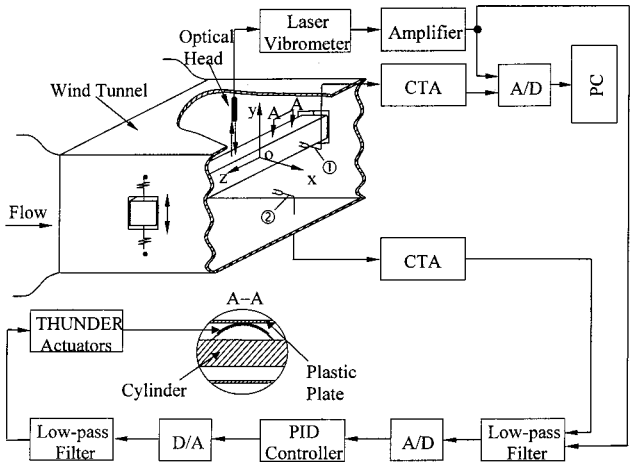

FIG. 1. Experimental setup. ① Monitor hot wire was located at $x=2h$, $y=1.5h$, $z=0$; ② feedback hot wire was located at $x=1.6h$, $y=-2.5h$, $z=0$.

which is the best feedback signal, flow or structural vibration or something else?

The present investigation pursues two objectives: (1) to improve the control system developed by Cheng *et al.*[8] and Zhang *et al.*[17] and find an optimum scheme to control fluid–structure interactions, and (2) to shed light upon the underlying physics of flow–structure interaction under external perturbation. Three control schemes, utilizing feedback signals from flow, structural vibration, or a combination of both, are considered and compared. The performances of the control schemes were assessed through measurements using a particle image velocimetry (PIV), laser-induced fluorescence (LIF) flow visualization, and laser Doppler anemometer (LDA). To understand the underlying physics, changes in spectral phase and coherence between flow and structural vibration due to the deployment of the control were investigated, along with the varying fluid damping of the fluid–structure system, which was evaluated from structural oscillation signals using an autoregressive moving average (ARMA) technique.

II. EXPERIMENTAL DETAILS

All experiments were performed in a closed-circuit wind tunnel with a square working section of 0.6 m×0.6 m and 2.4 m long, which has a uniform flow velocity up to 50 ms^{-1}. The free-stream turbulence intensity is less than 0.4%. More details of the tunnel were given in Zhou *et al.*[18] A square cylinder of height $h=15.2$ mm, flexibly supported on springs at both ends, was placed 0.2 m downstream of the exit plane of the tunnel contraction and allowed to vibrate laterally, as shown in Fig. 1. The free-stream velocity (U_∞) was adjusted to be about 3.58 ms^{-1}, corresponding to a Reynolds number, Re ($\equiv U_\infty h/\nu$, where ν is the kinematic viscosity)=3500. At this Re, resonance occurred, that is, the vortex shedding frequency f_s coincided with the natural frequency $f_n'(=30\,\mathrm{Hz})$ of the fluid-cylinder system, the maximum cylinder displacement, $Y_{\max}$, being about 1.2 mm or $0.08h$.

Details about the installation of the cylinder and characteristics of the actuators were given in Cheng *et al.*[8] As shown in Fig. 1, the upper side of the cylinder, parallel to the flow, was made of a thin plastic plate (13.8 mm×493 mm, 2/3 of the cylinder length) 3 mm thick, which was installed symmetrically about the midspan of the cylinder and flush with the rest of the cylinder surface. Three curved piezoelectric ceramic actuators were embedded in series in a slot underneath the plate. When placed within an electric field, the piezoelectric effect resulted in a strain in material. Under an applied voltage, the actuator deformed out of plane, driving the thin plate up and down and generating the desired surface perturbation.

The lateral structural displacement (Y) was measured by a laser vibrometer, which has a measurement uncertainty of about 0.5%. The laser beam was split into two, one monitoring the control performance and the other providing the feedback signal. The streamwise fluctuating velocity (u) was measured by two 5 μm tungsten wires, placed at $x/h=2$, $y/h=1.5$, and $z/h=0$ (hot wire ① in Fig. 1) and $x/h=1.6$, $y/h=-2.5$, and $z/h=0$ (hot wire ② in Fig. 1), respectively. The x, y, and z coordinates and their origin are defined in Fig. 1. Hot wires ① and ② were used to monitor the control performance and feedback signals, respectively. The choice of the feedback hot wire location may impact on the control performance. When the feedback hot wire is placed in the near wake, the signal is highly turbulent, thus affecting the control performance; further away from the wake such as at $x/h=1.6$ and $y/h=-2.5$, the coherent signal is dominant, which warrants a good control performance. The constant temperature circuit was used for the operation of the hot wires at an overheat ratio of 1.8. The feedback signals were low-pass filtered at a cutoff frequency of 200 Hz and then sent to a proportional-integral-derivative (PID) controller built-in with a 16-bit analog-to-digital (AD) and digital-to-analog converter. The signals were low-pass filtered again to remove the high frequency electronic noise (cutoff frequency =200 Hz) and amplified by two dual channel piezo driver amplifiers (Trek PZD 700) in order to drive the piezoelectric ceramic actuators. The signals, be they used for monitoring or feedback purposes, were conditioned and digitized using a 12-bit AD board at a sampling frequency of 3.5 kHz per channel. The duration of each record was about 20 s.

The LIF flow visualization and PIV measurements were conducted using a Dantec standard PIV2100 system. The digital particle images were taken by a charge coupled device camera (HiSense type 13, gain ×4, single for LIF or double frames for PIV, 1280×1024 pixels) and the illumination was given by two New wave standard pulsed laser sources of a wavelength of 532 nm, each having a maximum energy output of 120 mJ. A Dantec FlowMap Processor (PIV2100 type) was used to synchronize image taking and illumination. A wide-angle lens was used so that each image covered an area of 165 mm×125 mm or $x/h\approx 0.33-11.2$ and $y/h\approx -4.1-4.1$ of the flow field for LIF flow visualization and 155 mm×140 mm, i.e., $x/h\approx 0.6-10.8$, $y/h\approx -4.8-4.4$, for PIV measurements. Flow velocities, u and v, along the x and y direction, respectively, in the wake ($x/h=3$) were measured using a two-component LDA

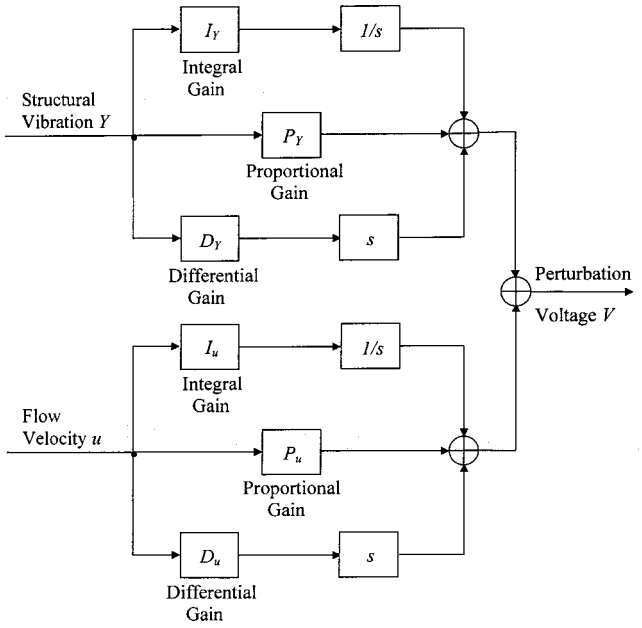

FIG. 2. Block diagram of PID control schemes.

system (Dantec Model 58N40 with an enhanced Flow Velocity Analyzer signal processor).

III. CONTROL SCHEMES AND CONTROLLER DESIGN

Three control schemes were considered depending on feedback signals used, namely, PID-Y, PID-u, and PID-Yu, referring to PID control using the Y signal measured by laser vibrometer, the u signal measured by hot wire ②, and the combination of the two signals, respectively. The controller was developed and implemented based on a dSPACE system, which had a real-time system for rapid control prototyping, production code generation, and hardware-in-the-loop tests. A digital signal processor (DSP) with SIMULINK function of MATLAB and software (ControlDesk 2.0) was used for sampling and processing feedback signals.

As illustrated in Fig. 2, the output of a PID controller is proportional to the sum of the input signal, its integral, and its derivative. The proportional gain (P), integral gain (I), and differential gain (D) of a PID controller can be individually or simultaneously adjusted. Each combination of the three quantities results in a different type of control. P control deploys a proportionally amplified input signal and has a limited success in obtaining a good performance in terms of steady-state errors, disturbance rejection, and transit response. A PI controller includes the integral of the input signal, and the steady-state error is eliminated at the expense of a larger transient overshoot and thus a further deterioration of the dynamic response. Once the derivative of the input signal is added, forming the PID controller, the system is able to provide an acceptable degree of error reduction along with an acceptable stability.[19] For each control scheme of PID-Y, PID-u, or PID-Yu, gain coefficients should be adjusted during experiments to achieve a maximum reduction in the amplitudes of Y and u. The tuning procedure was first to keep $I=D=0$ and vary P until the root-mean-square (rms) values, Y_{rms} and u_{rms}, of Y and u reached the minimum. Then I and D were successively added and adjusted until the optimal performance was achieved. The same procedure was followed for the three schemes, i.e., PID-Y, PID-u, and PID-Yu. Figure 3 shows the control performance versus each gain coefficient under different schemes. In the figure, the dashed line and dotted line corresponded to $u_{\mathrm{rms}}/U_\infty$ and Y_{rms}/h, respectively. Note that, for Yu-control, two sets of coefficients, (P_Y, I_Y, D_Y) and (P_u, I_u, D_u), are involved. It is evident that the PID controller outperforms the P and PI controllers. For all controllers, the Yu control has the best performance in terms of the reduction in Y_{rms} and u_{rms} followed by the u control and then the Y control. The difference in the control performance using different schemes is linked to the physical effect of each scheme on the fluid–structure system, which will be discussed in Sec. IV. It can also be seen that, irrespective of control schemes, P is much more effective than I or D in controlling vortex shedding and flow-induced vibration. P control generates a control action that is proportional to structural oscillation velocity ($\dot{Y}$) or flow velocity, thus physically causing a change in the system damping. Theoretically, the resonant flow–structure system was surely very sensitive to any damping variations. On the other hand, I and D controls are physically linked to displacement and acceleration feedback, respectively. The former has an impact upon the system stiffness, whereas the latter influences the effective mass. Both may in principle alter the natural frequency, f_n', of the system to some extent. However, this slight change in f_n' is probably not enough to generate any considerable effect on the strongly coupled vortex and structure synchronization, which occurs over the lock-on frequency range.[20]

The tuning process led to an optimal configuration for each scheme (PID control in Fig. 3) with the following parameters: $P_Y=1.2$, $I_Y=-0.3$, $D_Y=-0.0004$ for PID-Y, $P_u=3.5$, $I_u=0.2$, $D_u=0.0001$ for PID-u, and $P_Y=1.2$, $P_u=0.4$, $I_Y=0.2$, $I_u=0.2$, $D_Y=0.001$, $D_u=0.0001$ for PID-Yu. Unless otherwise stated, these parameters were used in experiments discussed hereinafter.

IV. PERFORMANCE OF VARIOUS CONTROL SCHEMES

Figure 4 compares the control performances of the three control schemes in terms of Y^*_{rms} and u^*_{rms}. Unless otherwise stated, the asterisk denotes the normalization by h and U_∞ in this paper. Compared to the unperturbed case, Y^*_{rms} and u^*_{rms} were reduced, respectively, by 40% and 17% using PID-Y, 53% and 32% using PID-u, and 82% and 70% using PID-Yu. Evidently, synchronizing vortex shedding and cylinder oscillation was greatly weakened in all cases. Nevertheless, PID-Yu overwhelms the other two schemes in performance, and PID-u considerably exceeds PID-Y. Cheng *et al.*[8] attempted to manipulate the same fluid–structure system using an open-loop control system. In their case, whether the flow or structural vibration was enhanced or impaired depended on the perturbation frequency (f_p). Both Y_{rms}/h and $u_{\mathrm{rms}}/U_\infty$ were reduced outside the synchronization range, i.e., $f_p^*=0.11-0.26$, but increased within the range. Further-

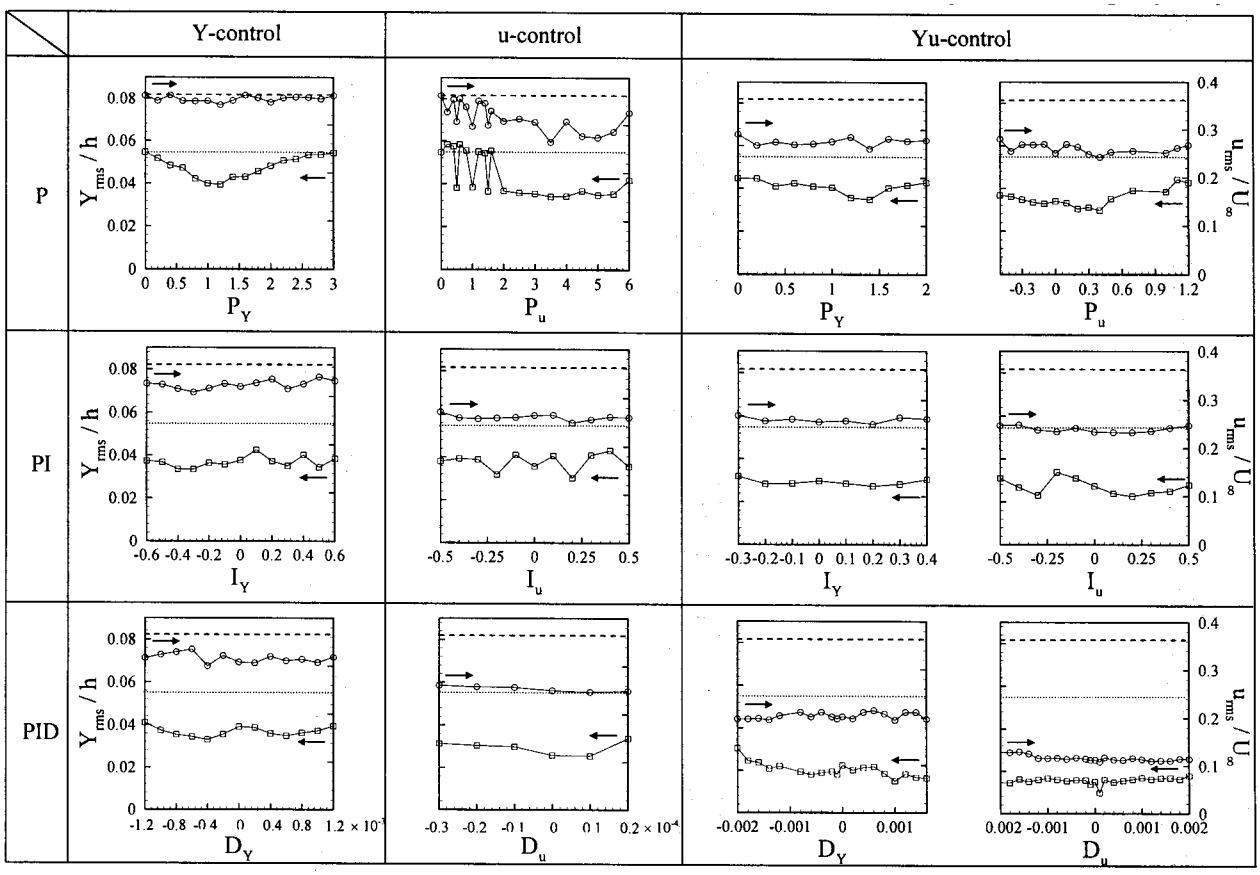

FIG. 3. Variation of $Y_{\rm rms}/h$ and $u_{\rm rms}/U_\infty$ with the proportional gain (P), integral gain (I), and differential gain (D) under different control schemes. · · · ·: unperturbed $Y_{\rm rms}/h$, and — — —: unperturbed $u_{\rm rms}/U_\infty$.

more, the maximum reduction was 75% in $Y_{\rm rms}/h$ and 68% in $u_{\rm rms}/U_\infty$, appreciably less than what was achieved by PID-Yu.

Typical photographs from flow visualization are presented in Fig. 5. The solid square in the figure denotes the cylinder position. The case without any external perturbation is given in Fig. 5(a) as a baseline for comparison. The best performed open-loop controlled case[8] when $f_p^*=0.1$ and $f_s^*=f_n'^*=0.13$ is also included. Figure 6 presents the isocontours of the normalized spanwise vorticity, $\omega_z^*=\omega_z h/U_\infty$, from the PIV measurement, which provide quantitative information on the performance of different control schemes, thus complementing flow visualization results. The experimental uncertainty of the vorticity measurement was estimated to be about 9%, close to the value of 10% reported by Sumner *et al.*[21] The unperturbed flow [Figs. 5(a) and 6(a)] displays the familiar Kármán vortex street. In the case of the open-loop control, the Kármán vortex street in Fig. 5(b) appears to be breaking up and the maximum vorticity level, $|\omega_{z\,\max}^*|$, in Fig. 6(b) drops by about 47%, compared with the unperturbed flow [Fig. 6(a)]. For the closed-loop control of PID-Y and PID-u schemes, the vortex street [Figs. 5(c) and 5(d) and Figs. 6(c) and 6(d)] is again breaking up, and the maximum vorticity level is not any lower than the open-loop case. In fact, the vorticity contours in the PID-Y and PID-u control scheme displays a higher level than that of the open-loop control. Once the PID-Yu scheme is applied, the control effect is strikingly enhanced; the flow-visualization photograph in Fig. 5(e) shows a radish-like wake instead of the Kármán vortex street. The magnitude of $|\omega_{z\,\max}^*|$ is reduced by 71% [Fig. 6(e)]. Note that the surface perturbation was imposed only on the upper side of the square cylinder. However, the wake below the centerline appears equally affected (Figs. 5

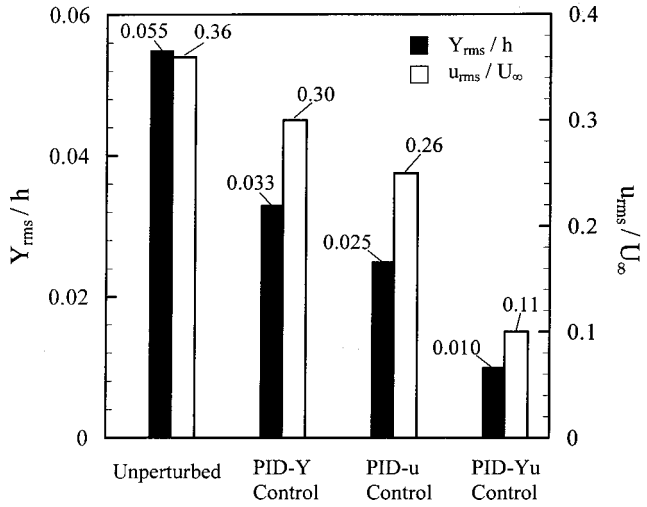

FIG. 4. Comparison in $u_{\rm rms}$ and $Y_{\rm rms}$ among various control schemes. The feedback and monitor hot wires were located at $x/h=1.6$, $y/h=-2.5$ and $x/h=2$, $y/h=1.5$, respectively.

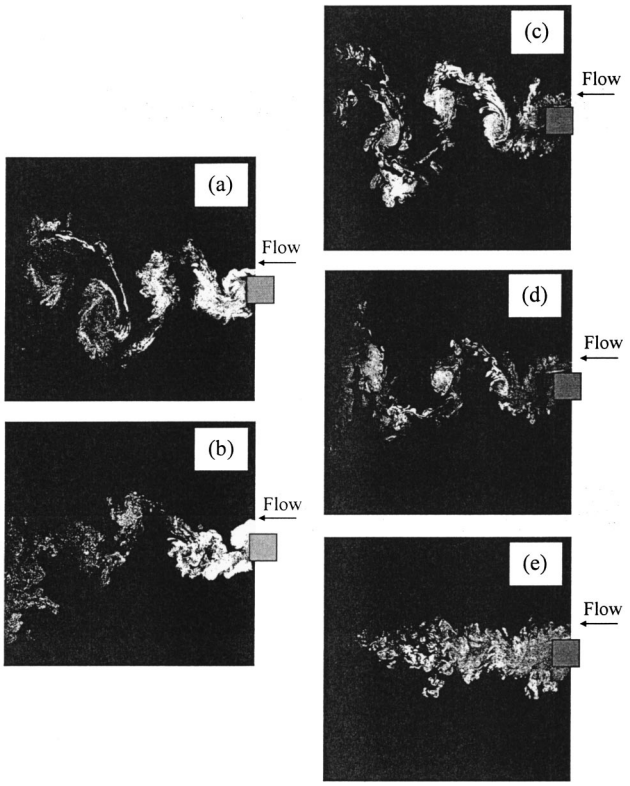

FIG. 5. Typical photographs from LIF flow visualization with and without control: (a) unperturbed; (b) open-loop control, $f_p^*=0.1$; (c) PID-Y; (d) PID-u; and (e) PID-Yu. The feedback and monitor hot wires were located at $x/h=1.6$, $y/h=-2.5$ and $x/h=2$, $y/h=1.5$, respectively.

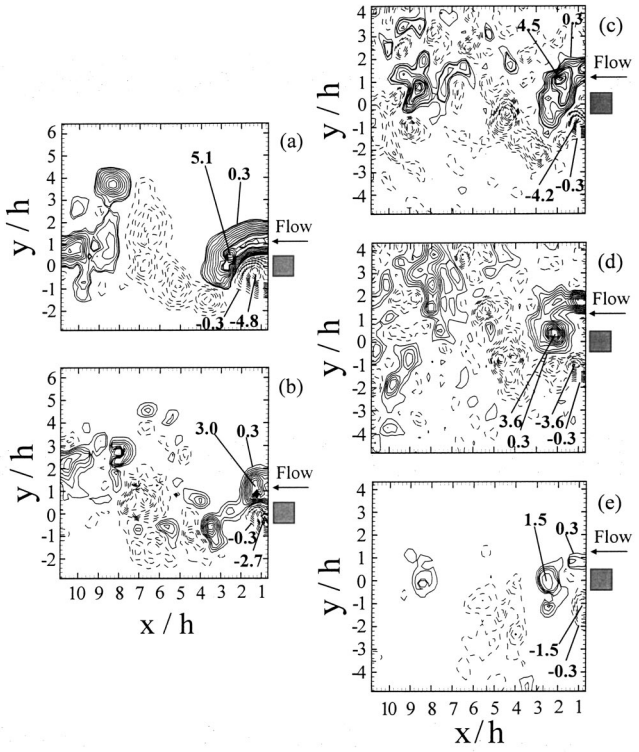

FIG. 6. PIV measured isocontours of spanwise vorticity $\omega_z^*=\omega_z h/U_\infty$ with and without control: (a) unperturbed; (b) open-loop control, $f_p^*=0.1$; (c) PID-Y; (d) PID-u; and (e) PID-Yu. The feedback and monitor hot wires were located at $x/h=1.6$, $y/h=-2.5$ and $x/h=2$, $y/h=1.5$, respectively.

and 6), similarly to Hsiao[3] and Huang.[11] The observation suggests that the present local perturbation has changed global interactions between fluid and structure.

Figure 7 presents the transition of the Y and u signals when the control action was switched on, which is evident from the variation of the actuating voltage (V_p). In all cases, there is a drastic reduction in the magnitude of Y or u once V_p was introduced. The most significant attenuation is obtained using PID-Yu [Fig. 7(c)], compared with the unperturbed case. It is of interest to compare the magnitudes of the actuating voltage in volts used in different schemes. The V_p magnitude is only 27 V for PID-Yu, but reaches 84 and 47 V in PID-Y and PID-u, respectively. Evidently, PID-Yu requires a lower actuating voltage and hence smaller perturbation amplitude than the other two schemes yet achieves a markedly better performance.

Figures 8(a) and 8(b) show the power spectral density functions, E_Y and E_u, of Y and u, respectively, with and without control. The spectrum of fluctuation α (α represents either Y or u) has been normalized such that $\int_0^\infty E_\alpha(f)df=1$. Without control, a pronounced peak occurs at $f_s^*=0.13$ in both E_Y and E_u, the number, 0.91 in E_Y and 0.59 in E_u, near the peak indicating the peak magnitude at f_s^*. Under the open-loop control ($f_p^*=0.1$), the peak magnitude at $f_s^*=0.13$ recedes by 75% in E_Y and 61% in E_u, compared with the unperturbed case. With the PID controllers applied, the peak magnitude in E_Y and E_u at f_s^* also retreats greatly, by 31% in E_Y and 19% in E_u for PID-Y and by 57% in E_Y and 44% in E_u for PID-u. Yet, the retreat is less than that achieved by the open-loop system. However, the PID-Yu scheme manages to reduce the peak magnitude by 87% in E_Y and 81% in E_u, showing a performance significantly superior to the open-loop system and other closed-loop schemes. Table I compares reductions in $E_{Y,\Delta f}^{(n)}$ and $E_{u,\Delta f}^{(n)}$ between different control schemes. $E_{Y,\Delta f}^{(n)}$ and $E_{u,\Delta f}^{(n)}$ ($n=1,2,3$) represent the energies of Y and u associated with the fundamental frequency (f_s^*, $n=1$), its second ($n=2$) and third ($n=3$) harmonics, respectively. $E_{Y,\Delta f}^{(n)}$ and $E_{u,\Delta f}^{(n)}$ were calculated by integrating their respective power spectrum density functions over 3 dB bandwidth with respect to the peak value. The open-loop control may reduce some harmonics more than PID-Y or PID-u does, and the PID-Yu control has the best performance of all, including the open-loop control. The difference in the control performance is attributed to different control signals. In the open-loop case, the control signal is independent of vortex shedding; in the closed-loop schemes the feedback signals from the fluid–structure interaction system are deployed. The observation indicates that the closed-loop control may not necessarily achieve a performance better than the open-loop control; the proper choice of the feedback signal is crucial. It is the combination of Y and u signals, not individual Y or u, which contains the information on fluid–structure interaction physics and thus warrants the best performance.

The overall performances of the three closed-loop con-

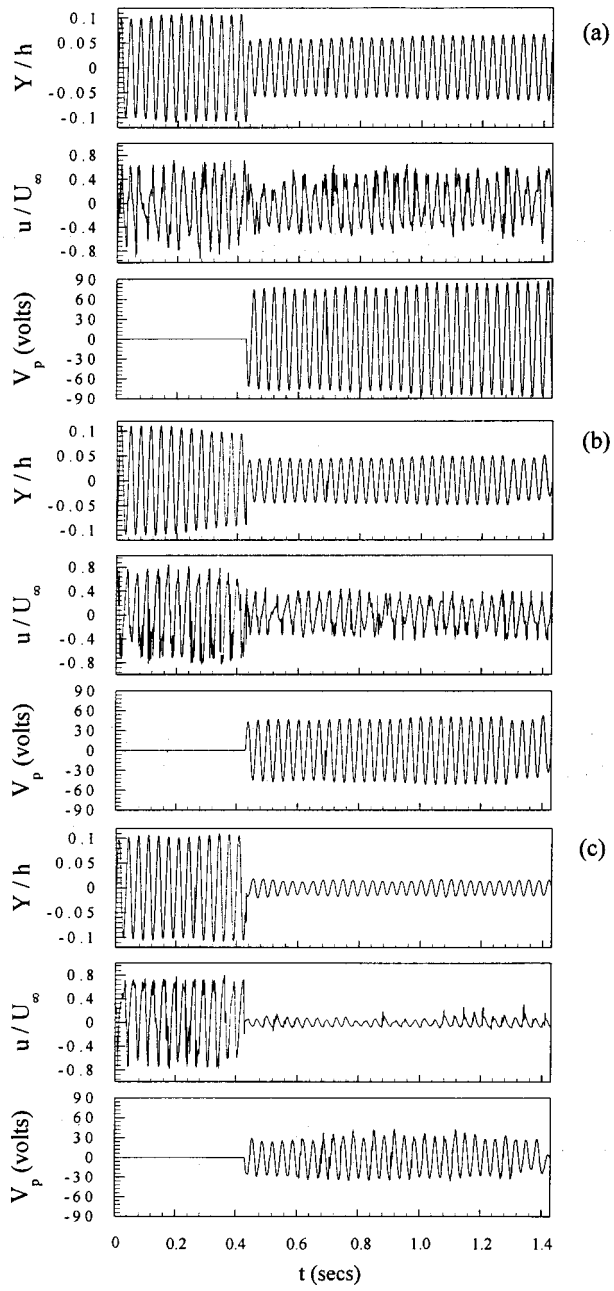

FIG. 7. Typical transition of structural vibration (Y), flow velocity (u), and perturbation voltage (V_p) signals when the PID controller was switched on. (a) PID-Y; (b) PID-u; and (c) PID-Yu. The feedback and monitor hot wires were located at $x/h=1.6$, $y/h=-2.5$ and $x/h=2$, $y/h=1.5$, respectively.

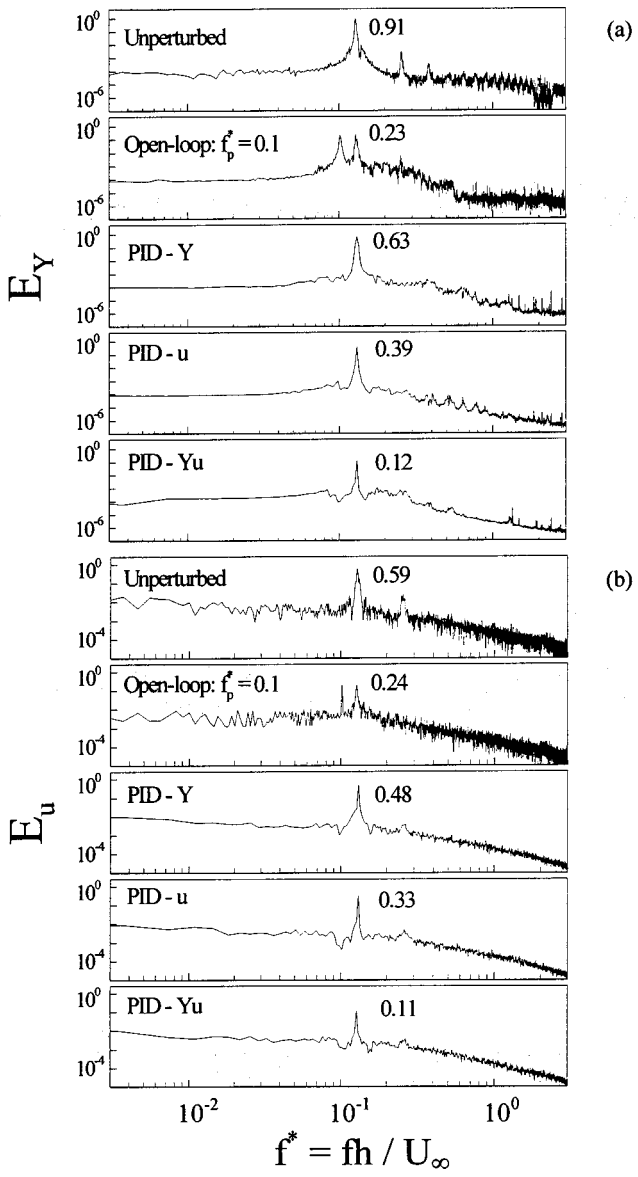

FIG. 8. Power spectra of structural vibration (Y) and flow velocity (u) with and without control: (a) E_Y and (b) E_u. The feedback and monitor hot wires were located at $x/h=1.6$, $y/h=-2.5$ and $x/h=2$, $y/h=1.5$, respectively.

trol schemes, together with open-loop control case ($f_p^*=0.1$), are summarized in Table II for comparison. Note that the control voltage, V_p, is a good indicator for the input control energy $W\,(=V_p^2/R$, where R represents the resistance of the actuators). Irrespective of the control schemes, R remains constant. Therefore a lower control voltage means a low energy requirement. The circulation (Γ) around a vortex is estimated by numerical integration $\Gamma^*=\Gamma/U_\infty h=\Sigma_{i,j}(\omega_z^*)_{ij}(\Delta A/h^2)$ (Brian and Donald[22]), where $(\omega_z^*)_{ij}$ is PIV-measured spanwise vorticity over area $\Delta A=\Delta x\Delta y$, Δx and Δy being the integral step along x and y directions, respectively. Integration was conducted over an area enclosed by the cutoff level $|\omega_{zc}^*|=0.3$, about 7% of $|\omega_{z\,\max}^*|$, which is the same as Brian and Donald[22] used. Errors associated with the Γ estimate were about 15%. It can be seen that PID-u control outperforms PID-Y control in every category, resulting in a higher reduction percentage in $Y_{\rm rms}/h$, $u_{\rm rms}/U_\infty$, and Γ despite smaller perturbation voltage amplitude. Among all control methods listed in Table II, PID-Yu has unequivocally the best performance in minimizing $Y_{\rm rms}^*$, $u_{\rm rms}^*$, and Γ^*. Its required actuating voltage V_p or the perturbation amplitude Y_p is only about 50%, 30%, and 20% of that used for PID-Y, PID-u, and the open-loop control ($f_p^*=0.1$), respectively. The result indicates one great advantage of the closed-loop control system over the open-loop one, i.e., the possibility to develop a more compact, self-contained and low energy control system, in particular, if the PID-Yu scheme is applied.

Figure 9 compares the cross-flow distributions of mean velocity U^* and Reynolds stresses $\overline{u^2}^*$, $\overline{v^2}^*$, and $\overline{uv}^*$ mea-

TABLE I. Reductions in $E^{(n)}_{Y,\Delta f}$ and $E^{(n)}_{u,\Delta f}$ associated with the first three harmonics of the vortex shedding frequency.

Control schemes		Open-loop $f_p^*=0.1$	PID-Y	PID-u	PID-Yu
$E^{(n)}_{Y,\Delta f}$	$E^{(1)}_{Y,\Delta f}$	77%↓	38%↓	68%↓	92%↓
	$E^{(2)}_{Y,\Delta f}$	57%↓	80%↓	82%↓	86%↓
	$E^{(3)}_{Y,\Delta f}$	49%↓	62%↓	69%↓	83%↓
$E^{(n)}_{u,\Delta f}$	$E^{(1)}_{u,\Delta f}$	65%↓	37%↓	64%↓	84%↓
	$E^{(2)}_{u,\Delta f}$	76%↓	59%↓	68%↓	83%↓
	$E^{(3)}_{u,\Delta f}$	72%↓	48%↓	67%↓	81%↓

sured by LDA at $x/h=3$ of the flows with and without perturbation. The closed-loop control using the PID-Y and PID-u schemes is not included since their performance is not any better than the open-loop control. For the open-loop control ($f_p^*=0.1$), the minimum $\overline{U}^*$ and maximum $\overline{u^2}^*$, $\overline{v^2}^*$, and $\overline{uv}^*$ show a considerable decrease, down to 85%, 85%, 88%, and 78% of that unperturbed, respectively. This was further reduced to 73%, 77%, 75%, and 71% of unperturbed case, respectively, for the closed-loop control using the PID-Yu scheme. The increased mean velocity deficit when the flow is perturbed is consistent with the decreased entrainment of high speed fluid from the free-stream due to the weakened vortex strength.[13] The reduced maximum $\overline{u^2}^*$, $\overline{v^2}^*$, and $\overline{uv}^*$ may be ascribed to the impaired vortex strength. It is pertinent to comment that $\overline{U}^*$, $\overline{u^2}^*$, $\overline{v^2}^*$, and $\overline{uv}^*$ are reasonably symmetric or antisymmetric about the centerline although the perturbation was imposed on the upper side only of the cylinder, internally consistent with the LIF flow visualization and PIV measured vortex street (Figs. 5 and 6).

The drag coefficient, C_D, was calculated based on the cross-flow distributions of $\overline{U}^*$, $\overline{u^2}^*$, and $\overline{v^2}^*$ (Ref. 23) in Fig. 9, viz.

$$C_D=2\int_{-\infty}^{\infty}\frac{\overline{U}}{U_\infty}\left(\frac{U_\infty-\overline{U}}{U_\infty}\right)d\left(\frac{y}{h}\right)+2\int_{-\infty}^{\infty}\left(\frac{\overline{v^2}-\overline{u^2}}{U_\infty^2}\right)d\left(\frac{y}{h}\right). \tag{1}$$

Without perturbation, C_D was 1.88, falling in the range of 1.7–2.0, as previously reported by, e.g., Lee,[24] Knisely,[25] and Zhou and Antonia.[26] C_D drops by 21.0% for the open-loop control and by 35.1% for the PID-Yu control. Hsiao and Shyu[3] observed a reduced C_D in an acoustically excited circular-cylinder wake. The observation was linked with a narrower wake and the smaller defect of mean velocity profile. The cross-flow distribution of $\overline{U}^*$ in Fig. 9(a) suggests

TABLE II. Control performance of various control schemes.

Control schemes	Open-loop $f_p^*=0.1$	PID-Y	PID-u	PID-Yu
Y_{rms}	75%↓	40%↓	53%↓	82%↓
u_{rms}	68%↓	17%↓	32%↓	70%↓
Γ	50%↓	22%↓	34%↓	65%↓
V_p	141.4 V	83.7 V	47.4 V	27.1 V
$Y_p/Y_{\max}$	35.1%	20.5%	14.7%	7.0%

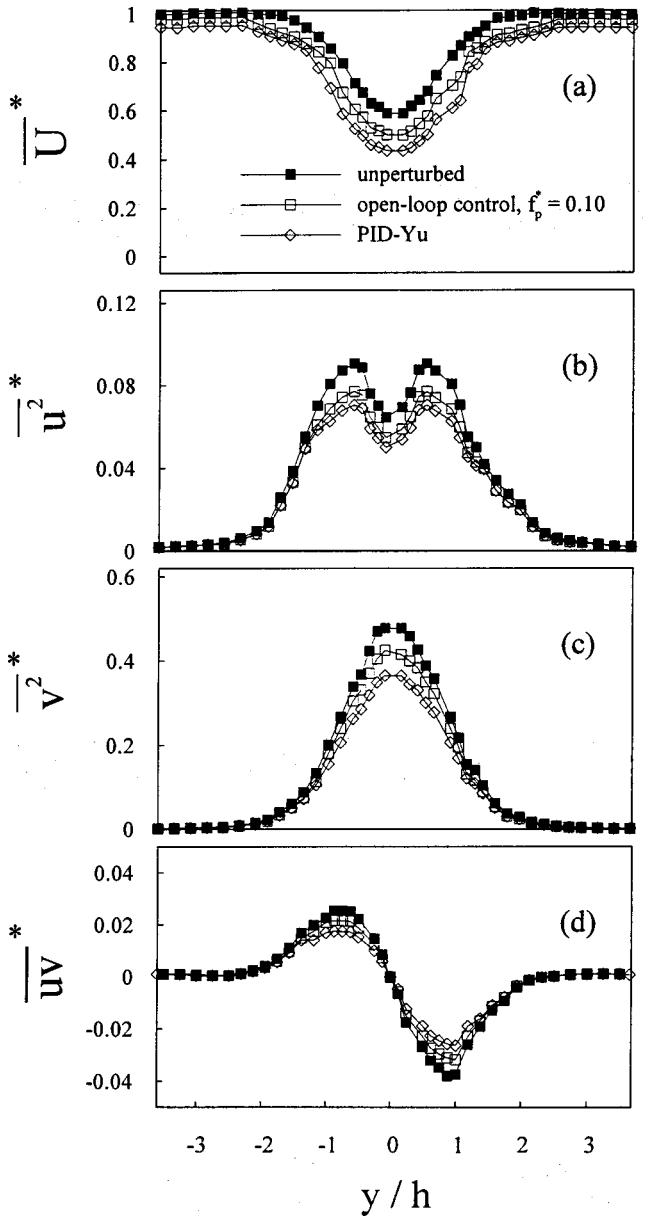

FIG. 9. Cross-flow distribution of mean velocity and Reynolds stresses at $x/h=3$ with and without control: (a) $\overline{U}^*$, (b) $\overline{u^2}^*$, (c) $\overline{v^2}^*$, and (d) $\overline{uv}^*$. The feedback and monitor hot wires were located at $x/h=1.6$, $y/h=-2.5$ and $x/h=2$, $y/h=1.5$, respectively.

an increasing wake width due to the perturbation on the cylinder. However, the maximum $\overline{u^2}^*$ and $\overline{v^2}^*$ are reduced because of the perturbation. It is therefore proposed that the perturbation leads to greatly weakened flow separation or vortex shedding and subsequently an increased backpressure. Consequently, C_D decreases.

V. DISCUSSIONS

To understand the physics behind impaired vortex shedding and structural vibration, the spectral phase shift (ϕ_{Yu}) and coherence (Coh_{Yu}) between vortex shedding and structural vibration are calculated from simultaneously measured Y and u using $\phi_{Yu}\equiv\tan^{-1}(Q_{Yu}/Co_{Yu})$ and $Coh_{Yu}=(Co_{Yu}^2+Q_{Yu}^2)/E_YE_u$, where Co_{Yu} and Q_{Yu} stand for the

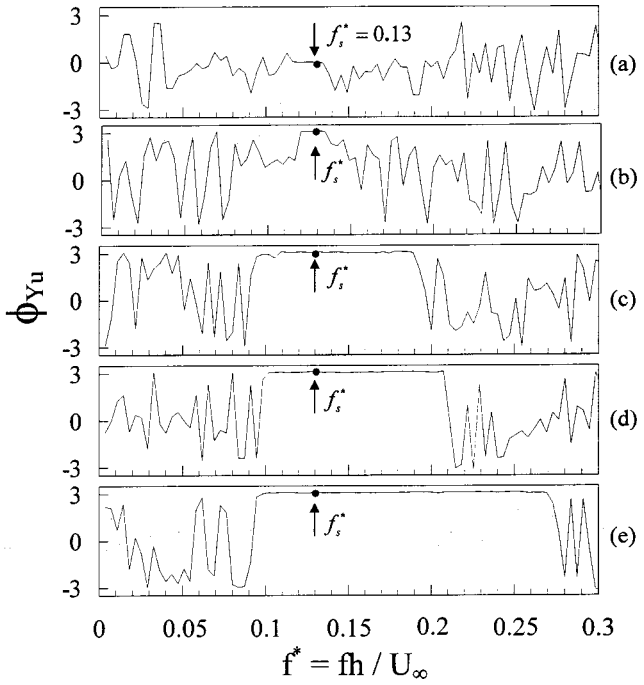

FIG. 10. Phase shift ϕ_{Yu} between structural displacement Y and fluctuating streamwise flow velocity u with and without control: (a) unperturbed; (b) open-loop control, $f_p^*=0.1$; (c) PID-Y; (d) PID-u; and (e) PID-Yu. The feedback and monitor hot wires were located at $x/h=1.6$, $y/h=-2.5$ and $x/h=2$, $y/h=1.5$, respectively.

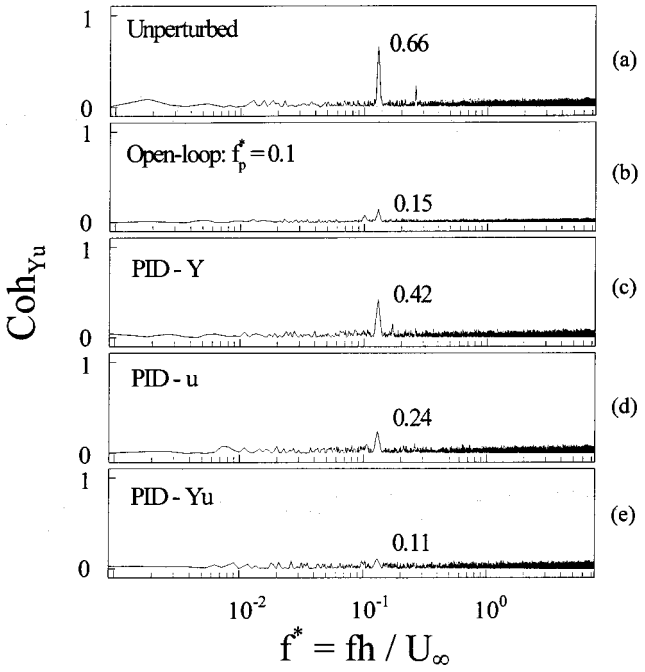

FIG. 11. Spectral coherence Coh_{Yu} between structural displacement Y and fluctuating streamwise flow velocity u with and without control. The feedback and monitor hot wires were located at $x/h=1.6$, $y/h=-2.5$ and $x/h=2$, $y/h=1.5$, respectively.

cospectrum and quadrature spectrum of Y and u, respectively. Coh_{Yu} provides a measure of the degree of correlation between the Fourier components of Y and u. A fast Fourier transform (FFT) scheme (e.g., Zhang *et al.*[27]) is used for spectral calculation. Cheng *et al.*'s analysis indicated that ϕ_{Yu} at f_s^* approximately described the phase relationship between the coherent lateral velocity, v, of the flow around the cylinder and the lateral structural oscillating velocity, $\dot{Y}$, its zero and π values corresponding to synchronization and the opposite movement between $\dot{Y}$ and v, respectively. Without perturbation, ϕ_{Yu} is zero near $f_s^*=0.13$ [Fig. 10(a)], consistent with synchronizing vortex shedding and structural vibration. The plateau about f_s^* indicates the synchronizing Y and u signals over a range of frequencies. Once perturbed using the open-loop control ($f_p^*=0.1$), ϕ_{Yu} was changed from 0 to π in a narrow frequency range about f_s^* [Fig. 10(b)]. This implies a change in the nature of the fluid–structure interaction, that is, the synchronizing v and $\dot{Y}$ turn into antiphased interactions against each other. As a result, Coh_{Yu} at f_s^* recedes from 0.65 to 0.15 [Figs. 11(a) and 11(b)]. The drastic reduction in Coh_{Yu} means a decoupled correlation between vortex shedding and structural vibration. With closed-loop controls deployed, ϕ_{Yu} about f_s^* again shifts from 0 to π, which is evident in Figs. 10(c)–10(e). It is noteworthy that the frequency range over which $\phi_{Yu}=\pi$ exceeds markedly that in the open-loop control. This frequency range is largest for PID-Yu, from 0.11 to 0.27 [Fig. 10(e)], essentially covering the entire frequency range (0.11–0.26) of synchronization between vortex shedding and induced vibration for bluff bodies with fixed separation points.[20] Any excitation force falls in this frequency range may lead to the synchronization phenomenon. The observation suggests that PID-Yu has completely altered the phase relationship between v and $\dot{Y}$ from in-phase to antiphase, whereas other schemes have done it over a small range of frequencies about f_s^*. In correspondence to the changing phase between vortex shedding and structural vibration, the peak at f_s^* in Coh_{Yu} [Figs. 11(c)–11(e)] retreats, compared with the unperturbed flow, and in effect completely vanishes when PID-Yu is deployed.

The jump in ϕ_{Yu} from 0 to π is associated with greatly impaired vortex shedding and structural vibration. It may be inferred that the fluid–structure system damping must be changed. Damping models the energy dissipation of the system during vibrations and plays an important role in the stability of a structure and its vibration amplitude. The synchronizing vortex shedding and structural oscillation will be effectively attenuated if the damping ratio of the system is increased. It is therefore worthwhile examining how the system damping ratio has been altered due to the introduction of control. In this paper, we define the effective damping, representing the energy dissipation of a system, as the sum of structural damping and fluid damping. The former may be generated by material, friction, impacting, and the rubbing of two surfaces in contact, while the latter results from skin friction and viscous dissipation, i.e., viscous shearing of a fluid at the surface of the structure and flow separation.[28] Fluid damping is motion-dependent and is difficult to estimate. Zhou *et al.*[29] and Zhang *et al.*[30] used an autoregressive moving average (ARMA) technique to calculate the effective damping ratios from measured displacement time series. Interested readers may refer to their papers for more details of

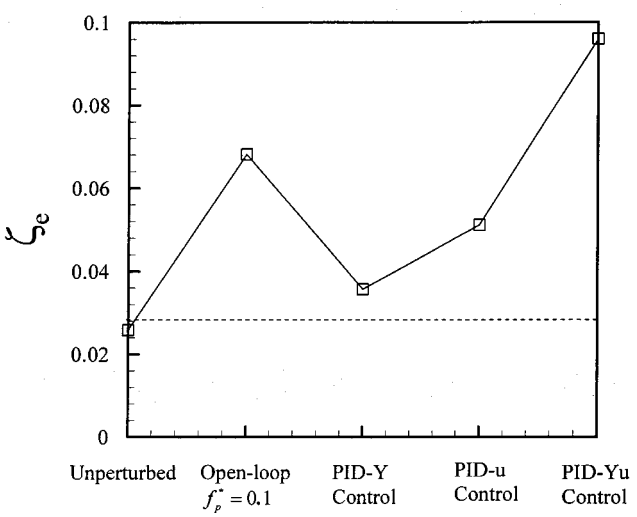

FIG. 12. Effect of open- and closed-loop control on cross-flow effective damping ratios, ζ_y. The dashed line denotes the structural damping ratio ζ_s measured without flow.

the technique. This technique is used presently to estimate the effective damping ratio ζ_e from the measured Y signal. The ARMA models of an order of 190 and 70 000 data points were used for calculation. Figure 12 shows ζ_e for different schemes. The structural damping ratio ζ_s of the first-mode motion, indicated by a dashed line in the figure, was measured under no-flow condition with the cylinder excited by an electromechanical shaker. Without perturbation, vortex shedding synchronizes with structural vibration, and ζ_e is less than ζ_s, albeit slightly. This suggests a negative fluid damping ratio ζ_f since $\zeta_e = \zeta_s + \zeta_f$. The negative ζ_f simply means that vortex shedding enhances the structural vibration.[29,30] For the open-loop control ($f_p^* = 0.1$), ζ_e increases by 163.2%, compared with the unperturbed case. Similarly, the closed-loop control using PID-Y, PID-u, and PID-Yu leads to an increase in ζ_e by 37.9%, 97.7%, and 271.4%, respectively.

Vortex-induced vibrations originate from fluid excitation forces, which are created by vortex shedding from a bluff body. The forces cause the structure to vibrate. The resultant structural vibrations may in turn influence the flow field, giving rise to fluid–structure coupling and even resonance when the frequency of the forces/vortex shedding can be appreciably modified[29] and the structural vibration can be grossly amplified. The coupling is in general a highly nonlinear function of both structural motion and flow velocity. In the open-loop control, the control signal is a periodic signal, which is independent of fluid–structure interactions. However, when the control signal frequency is outside the synchronization range, i.e., $f_p^* = 0.11 - 0.26$, the control effect may alter the nature of the fluid–structure coupling, changing the in-phased fluid–structure synchronization into antiphased interactions between fluid and structure.[8] Meanwhile, the effective damping ratio of the system increases significantly, enhancing the dissipation of both vortex shedding and structural vibration energies. As such, the nature of fluid and structure interactions has been changed from reinforcing each other into moving against each other. This change in the physical interaction causes drastically weakened vortex shedding and hence structural vibration. For the PID-u closed-loop scheme, the feedback signal is from flow, which is the excitation source. Therefore the effect of the control action is to modify directly the flow excitation and subsequently or indirectly the structural vibration. This control system allows the phase relationship between vortex shedding and structural vibration to be varied, either in-phased or antiphased, or something between. In the antiphased case, the control effect again alters the in-phased fluid–structure synchronization into antiphased interactions between fluid and structure, thus reducing effectively vortex shedding strength and structural vibration. Nevertheless, with an input energy of one-third (Table II) of that applied in the open-loop case, its performance is not necessarily better than the open-loop control. Similarly, the PID-Y control can reduce effectively the vortex shedding strength and structural vibration. However, this scheme uses the structural vibration signal as the feedback signal, that is, the feedback information reflects the passive response of fluid–structure interactions, instead of the excitation source. Consequently, the control performance is less effective than the PID-u scheme, even though the input energy has nearly doubled that of the PID-u scheme. For the PID-Yu scheme, the feedback signal is a combination of both Y and u signals and reflects both excitation consequence and source, and perhaps more importantly reflects the interaction/coupling between flow excitation and structural vibration, addressing the essence that amplifies both structural vibration and vortex shedding. As a result, this scheme has a superior performance to all other schemes, even with an input energy of 19%. 32%, and 57% of those applied in the open-loop, PID-u, and PID-Y schemes, respectively.

VI. CONCLUSIONS

The closed-loop control using PID controllers is developed to suppress vortex shedding and vortex-induced vibration on a flexibly supported square cylinder. The control is made possible using piezoelectric ceramic actuators to perturb one surface of the cylinder. Three control schemes are investigated, including PID-Y, -u, and -Yu, each deploying one different feedback signal. The investigation leads to the following conclusions.

(1) The presently developed flow control effectively turns the in-phased vortex shedding and structural vibration into the antiphased. This is associated with a significant increase in the effective damping ratio of the flow–structure system, implying an enhanced dissipation of vortex shedding and structural vibration energies. As a result, both vortex strength and structural vibration amplitude are remarkably reduced, and their correlation appears diminished. The drag coefficient is also greatly reduced.

(2) The PID-Yu scheme, with the least input energy required, has the best performance of all, including the open-loop control; the visualized wake appears radish-like, suggesting an almost complete destruction of the Kármán vortex street. Such a performance is attributed to its control signal, which is the combination of flow excitation and structural vibration, thus reflecting the nonlinear interactions between

fluid and structure. The PID-*u* control scheme outperforms the PID-*Y* strategy. While the latter targets the control of passive structural vibration, the former directly tackles the fluctuating flow, which is the origin of the excitation forces on structural vibration, thus being more effective. However, with a small input energy, compared with that applied in the open-loop system, the performance of the two closed-loop schemes is not necessarily better than that of the open-loop control. The observation points to a crucial role the feedback signal plays in the closed-loop control of flow or flow-induced vibrations.

(3) The closed-loop control has many advantages over an open-loop system. The open-loop control depends on the perturbation frequency f_p^*; it can only suppress vortex shedding or structural vibration if f_p^* is outside the synchronization range. Within the synchronization range, the open-loop control enhances vortex shedding or structural vibration. On the other hand, with the feedback signal from flow, structural vibration, or a combination of both, the closed-loop control can always suppress both vortex shedding and structural vibration. Furthermore, with the deployment of a closed-loop control, the required perturbation amplitude or voltage can be greatly reduced, pointing to the possibility of developing a more compact and self-contained control system.

ACKNOWLEDGMENTS

The authors wish to acknowledge support given to them by the Central Research Grant of The Hong Kong Polytechnic University through Grant No. G-W108 and a grant from Research Grants Council of Hong Kong Special Administrative Region, China (Project No. PolyU 5294/03E).

[1]M. M. Zdravkovich, ''Review and classification of various aerodynamic and hydrodynamic means for suppressing vortex shedding,'' J. Wind. Eng. Ind. Aerodyn. **7**, 145 (1981).
[2]D. M. Bushnell and J. N. Hefner, ''Viscous drag reduction in boundary layers,'' *Progress in Aeronautics and Astronautics* (AIAA, Washington, D.C., 1990), Vol. 123.
[3]F. B. Hsiao and J. Y. Shyu, ''Influence of internal acoustic excitation upon flow passing a circular cylinder,'' J. Fluids Struct. **5**, 427 (1991).
[4]O. M. Griffin and S. E. Ramberg, ''Vortex shedding from a cylinder vibrating in line with an incident uniform flow,'' J. Fluid Mech. **75**, 257 (1976).
[5]P. W. Bearman, ''Vortex shedding from oscillating bluff bodies,'' Annu. Rev. Fluid Mech. **16**, 195 (1984).
[6]B. Protas and J. E. Wesfreid, ''Drag force in the open-loop control of cylinder wake in the laminar regime,'' Phys. Fluids **14**, 810 (2002).
[7]D. R. Williams, H. Mansy, and C. Amato, ''The response and symmetry properties of a cylinder wake subjected to localized surface excitation,'' J. Fluid Mech. **234**, 71 (1992).
[8]L. Cheng, Y. Zhou, and M. M. Zhang, ''Perturbed interaction between vortex shedding and induced vibration,'' J. Fluids Struct. **17**, 887 (2003).
[9]J. E. Ffowcs Williams and B. C. Zhao, ''The active control of vortex shedding,'' J. Fluids Struct. **3**, 115 (1989).
[10]K. Roussopoulos, ''Feedback control of vortex shedding at low Reynolds numbers,'' J. Fluid Mech. **248**, 267 (1993).
[11]X. Y. Huang, ''Feedback control of vortex shedding from a circular cylinder,'' Exp. Fluids **20**, 218 (1996).
[12]E. Berger, ''Suppression of vortex shedding and turbulence behind oscillating cylinders,'' Phys. Fluids **10**, 191 (1967).
[13]H. M. Warui and N. Fujisawa, ''Feedback control of vortex shedding from a circular cylinder by cross-flow cylinder oscillations,'' Exp. Fluids **21**, 49 (1996).
[14]P. T. Tokumaru and P. E. Dimotakis, ''Rotary oscillation control of a cylinder wake,'' J. Fluid Mech. **224**, 77 (1991).
[15]J. R. Filler, P. L. Marston, and W. C. Mih, ''Response of the shear layers separating from the circular cylinder to small amplitude rotational oscillations,'' J. Fluid Mech. **231**, 481 (1991).
[16]A. Baz and J. Ro, ''Active control of flow-induced vibrations of a flexible cylinder using direct velocity feedback,'' J. Sound Vib. **146**, 33 (1991).
[17]M. M. Zhang, L. Cheng, and Y. Zhou, ''Closed-loop control of fluid–structure interactions on a flexibly supported cylinder,'' Eur. J. Mech. B/Fluids **23**, 189 (2004).
[18]Y. Zhou, H. J. Zhang, and M. W. Yiu, ''The turbulent wake of two side-by-side circular cylinders,'' J. Fluid Mech. **458**, 303 (2002).
[19]G. Franklin, J. David Powell, and M. Workman, *Digital Control of Dynamics Systems* (Addison-Wesley, Reading, MA, 1998).
[20]B. H. L. Gowda, ''Some measurements on the phenomenon of vortex shedding and induced vibrations of circular cylinders,'' *Deutsche Luft- und Raumfahrt Forschungsbericht*, No. 75-01 (1975) [English translation: *Germany Aerospace and Aeronautical Research Report*].
[21]D. Sumner, S. J. Price, and M. P. Païdoussis, ''Flow-pattern identification for two staggered circular cylinders in cross-flow,'' J. Fluid Mech. **411**, 263 (2000).
[22]C. Brian and C. Donald, ''An experimental study of entrainment and transport in the turbulent near wake of a circular cylinder,'' J. Fluid Mech. **136**, 321 (1983).
[23]R. A. Antonia and S. Rajagopalan, ''A comment on the determination of drag of a circular cylinder,'' AIAA J. **28**, 1833 (1990).
[24]B. E. Lee, ''The effect of turbulence on the surface pressure field of a square prism,'' J. Fluid Mech. **69**, 263 (1975).
[25]C. W. Knisely, ''Strouhal numbers of rectangular cylinders at incidence—A review and new data,'' J. Fluids Struct. **4**, 371 (1990).
[26]Y. Zhou and R. A. Antonia, ''Effect of initial conditions on structures in a turbulent near-wake,'' AIAA J. **32**, 1207 (1994).
[27]H. J. Zhang, Y. Zhou, and R. A. Antonia, ''Longitudinal and spanwise structures in a turbulent wake,'' Phys. Fluids **12**, 2954 (2000).
[28]R. D. Blevins, *Flow-Induced Vibration* (Krieger, Malabar, FL, 1994).
[29]Y. Zhou, Z. J. Wang, R. M. C. So, S. J. Xu, and W. Jin, ''Free vibrations of two side-by-side cylinders in a cross flow,'' J. Fluid Mech. **443**, 197 (2001).
[30]H. J. Zhang, Y. Zhou, R. M. C. So, M. P. Mignolet, and Z. J. Wang, ''A note on the fluid damping of an elastic cylinder in a cross-flow,'' J. Fluids Struct. **17**, 479 (2003).